Geoderma 195–196 (2013) 1–11

Contents lists available at SciVerse ScienceDirect

Geoderma

journal homepage: www.elsevier.com/locate/geoderma

Uncovering patterns of near-surface saturated hydraulic conductivity in an overland flow-controlled landscape

Alexander Zimmermann [a,*], Dustin S. Schinn [a], Till Francke [a], Helmut Elsenbeer [a,b], Beate Zimmermann [a]

[a] Institute of Earth and Environmental Science, University of Potsdam, Karl-Liebknecht-Str. 24-25, 14476 Potsdam, Germany
[b] Smithsonian Tropical Research Institute, Apartado 0843-03092, Balboa, Ancón, Panama

ARTICLE INFO

Article history:
Received 2 March 2012
Received in revised form 18 October 2012
Accepted 11 November 2012
Available online 9 December 2012

Keywords:
Soil hydrology
Saturated hydraulic conductivity
Overland flow generation
Spatial patterns
Drainage network

ABSTRACT

Saturated hydraulic conductivity (K_s) is an important soil characteristic affecting soil water storage, runoff generation and erosion processes. In some areas where high-intensity rainfall coincides with low K_s values at shallow soil depths, frequent overland flow entails dense drainage networks. Consequently, linear structures such as flowlines alternate with inter-flowline areas. So far, investigations of the spatial variability of K_s mainly relied on isotropic covariance models which are unsuitable to reveal patterns resulting from linear structures. In the present study, we applied two sampling approaches so as to adequately characterize K_s spatial variability in a tropical forest catchment that features a high density of flowlines: A classical nested sampling survey and a purposive sampling strategy adapted to the presence of flowlines. The nested sampling approach revealed the dominance of small-scale variability, which is in line with previous findings. Our purposive sampling, however, detected a strong spatial gradient: surface K_s increased substantially as a function of distance to flowline; 10 m off flowlines, values were similar to the spatial mean of K_s. This deterministic trend can be included as a fixed effect in a linear mixed modeling framework to obtain realistic spatial fields of K_s. In a next step we used probability maps based on those fields and prevailing rainfall intensities to assess the hydrological relevance of the detected pattern. This approach suggests a particularly good agreement between the probability statements of K_s exceedance and observed overland flow occurrence during wet stages of the rainy season.

1. Introduction

The saturated hydraulic conductivity (K_s) exerts a dominating influence on the partitioning of rainfall in vertical and lateral flow paths. Therefore, estimates of K_s are essential for describing and modeling hydrological processes. For such applications, it might be beneficial to characterize not only the frequency distribution of K_s but also its spatial structure as the spatial organization of soil properties, among them K_s, strongly influences runoff generation (Herbst et al., 2006; Merz and Bárdossy, 1998; Merz and Plate, 1997; Mueller et al., 2007; Taskinen et al., 2008). According to the majority of studies which investigated spatial correlations of K_s, the size of the area of interest determines whether long-range or short-range autocorrelation dominates (Zimmermann et al., 2008). In large research areas, the variation of K_s is dominated by long-range processes associated with differences in parent material and land use (Cemek et al., 2007; Iqbal et al., 2005). In smaller areas, which are homogeneous with respect to these factors, the predominant short-range autocorrelation of K_s (Duffera et al., 2007; Mallants et al., 1996; Mohanty et al., 1991; Sobieraj et al., 2004; Zimmermann and Elsenbeer, 2008) is attributed to local variations in soil structure (Mohanty et al., 1991; Sobieraj et al., 2004). In the latter situation, the spatial prediction of K_s values at unsampled locations is extremely difficult due to the large kriging variance in between measurement locations.

In addition to the variability across spatial domains, K_s shows pronounced changes with soil depth. In the majority of cases, mean K_s decreases with increasing soil depth (e.g. Ahuja et al., 1984; Bonell et al., 1981; Chappell and Sherlock, 2005; Ziegler et al., 2004; Zimmermann and Elsenbeer, 2008), a decrease some attribute to higher clay contents or a lower biogenic macroporosity in subsurface (>0.2 m depth) compared to surface (0–0.2 m depth) soil layers (e.g. Ahuja et al., 1984; Bonell et al., 1981). In areas where a pronounced decrease of K_s at a shallow depth coincides with the occurrence of large and intense rainfall events, saturation-excess overland flow occurs frequently (Bonell and Gilmour, 1978; de Moraes et al., 2006; Elsenbeer and Vertessy, 2000; Germer et al., 2010). Interestingly, several of the aforementioned studies described a runoff mechanism distinct from that of other well-known overland flow-prone catchments (e.g. Dunne and Black, 1970a, 1970b): in areas with extensive near-surface impeding layers, overland flow may essentially be "widespread" (Bonell and Gilmour, 1978), whereas overland flow which originates as a consequence of a near-stream water table rise is restricted to relatively small (downslope) areas (Dunne and Black, 1970a, 1970b). Studies

* Corresponding author. Tel.: +49 331 977 2047; fax: +49 331 977 2068.
E-mail address: alexander.zimmermann.ii@uni-potsdam.de (A. Zimmermann).

0016-7061/$ – see front matter © 2012 Elsevier B.V. All rights reserved.
http://dx.doi.org/10.1016/j.geoderma.2012.11.002

following the investigation of Bonell and Gilmour (1978) modified the notion of "widespread" in that overland flow can be pervasive on a hillslope yet restricted to certain microtopographic features such as flowlines and swales (Bonell et al., 1981; Elsenbeer and Vertessy, 2000; Loos and Elsenbeer, 2011).

Spatially organized overland flow on hillslopes, however, hardly agrees with an uncorrelated K_s pattern although the latter might be expected on slopes with homogeneous soil and vegetation cover (see first part of this section). In fact, it is more likely that the pattern of K_s reflects the spatial organization of overland flow, or vice versa. To overcome the apparent mismatch between reported K_s patterns and hydrological observations we hypothesized that K_s varies as a function of distance to flowline.

The main objective of our study is to test this hypothesis. Moreover, we wish to illustrate how prior hydrological knowledge (in our case the position of flowlines) can be used to uncover K_s patterns. Finally, we wish to place our data into a hydrological context to inform studies which apply distributed hydrological models on the hillslope to small catchment scale (e.g. Herbst et al., 2006; Merz and Bárdossy, 1998; Weiler and McDonnell, 2004). To achieve our aims, we modeled K_s spatial variability in an overland flow-prone forest catchment (Godsey et al., 2004; Zimmermann et al., 2012) following two different sampling approaches: in a first step, we employed a nested spatial sampling design (Youden and Mehlich, 1937) which reveals the spatial scales where most variation occurs. This or similar sampling approaches are standard and have been applied in several of the aforementioned K_s studies. Our motivation to employ nested spatial sampling was to test its suitability to uncover the hypothesized K_s pattern. In a second step, we applied a purposive sampling strategy adapted to the presence of flowlines. If K_s were indeed linked to the preferential occurrence of overland flow in flowlines, the second approach should clearly reveal a discernible spatial pattern. Finally, we combined the datasets and performed spatial predictions of K_s in order to assess the hydrological relevance of the detected K_s patterns.

2. Methods

2.1. Study site

The study site, Lutzito catchment (LC from hereon), is a 3.3 ha catchment located on Barro Colorado Island (BCI), Panama (9° 9′ 32″ N, 79° 50′ 17″ W; Fig. 1a,b). The island was isolated from the main land in 1914 after damming the Chagres River to form Lake Gatun, which is part of the Panama Canal. The topography of LC is heterogeneous: channels and rills dissect slopes that reach 35° in places. Most of the slopes in LC feature flowlines, which drain into the channel network (Fig. 1c,d; see also Video 1, Supplementary material).

The vegetation of BCI has been classified as tropical semideciduous moist forest (Foster and Brokaw, 1982). The forest in LC is secondary growth older than 100 years (Foster and Brokaw, 1982; Kenoyer, 1929).

The climate features distinct wet and dry seasons. The wet season lasts from May to mid-December. Total annual rainfall averages 2641 ± 485 mm (mean $\pm$ 1 sd, n = 82, data from 1929 to 2010, courtesy of the Environmental Sciences Program, Smithsonian Tropical Research Institute, Republic of Panama). Long-term averages of monthly rainfall indicate a fairly uniform rainfall distribution during the wet season with a maximum of around 400 mm in November. There is, however, a large year-to-year variation, and pronounced dry spells are common during the wet season.

LC is underlain by tuffaceous siltstone of the Caimito Marine Facies (Woodring, 1958). Soils are classified as Eutric Cambisols (F.A.O., 1998) or, following USDA criteria (Soil Survey Staff, 2006), as Typic Eutrudepts (Baillie et al., 2007) and reach depths between 0.3 m on some ridges and steep slopes and ~1 m elsewhere. Data of a recent soil survey (Baillie et al., 2007) suggest a characteristic sequence of soil texture in our research area: silty loams and clay loams prevail at a depth of 0–5 cm, silty clays occur at depths of 5–40 cm, and clay loams occupy the bottom of the soil profile (40–75 cm).

At the end of the dry season (May) and to a lesser extent during prolonged dry periods (June–July), soils in LC show cracks up to 2 cm wide and 10 cm deep (Dietrich et al., 1982) due to a substantial admixture of smectite in the clay fraction (Grimm et al., 2008). During the progressing wet season, cracks close and the degree of saturation (i.e. wetness) in the upper soils increases to more than 60% (Zimmermann et al., 2012). The spatial mean of infiltrability exceeds rainfall intensities substantially (Zimmermann et al., 2012); there is, however, evidence for a strong decrease of K_s with depth (Godsey et al., 2004; Zimmermann et al., 2012). Given the prevailing rainfall characteristics and soil moisture conditions during the wet season, this depth gradient of K_s likely results in a near-surface perched water table and explains observations of frequent saturation-excess overland flow (Dietrich et al., 1982; Godsey et al., 2004; Loos and Elsenbeer, 2011; Zimmermann et al., 2012).

2.2. K_s measurements

Undisturbed soil samples were taken in the wet season of 2009 and 2010 using a drop hammer method on leveled ground. The core cylinders were 3.65 cm and 6 cm in radius and height, respectively. After cutting the core ends level with a sharp knife we slowly saturated the samples upside down for a period of 48 h to prevent air entrapment (Reynolds et al., 2002). Subsequently, we applied a constant water head and recorded the flow rate through the cores per time unit, following the methodology described by Reynolds et al. (2002). After establishing a constant flow rate we measured percolated water volume per time unit and calculated K_s according to Darcy's equation for saturated conditions:

$$q = -K_s\left(\frac{dh}{ds}\right) \quad (1)$$

where q refers to the flux density (m s^{-1}), K_s is the saturated hydraulic conductivity (m s^{-1}), and dh/ds is the hydraulic gradient (m m^{-1}). The flux density can be expressed as $q = Q/A$ with Q being the water flux (m^3 s^{-1}) and A the cross section the water flows through (m^2).

2.3. Sampling approaches

2.3.1. Nested spatial sampling approach

We chose an unbalanced nested sampling design (Oliver and Webster, 1987; Youden and Mehlich, 1937) to explore the spatial structure of K_s in Lutzito catchment. Nested sampling was adapted from multi-stage hierarchical sampling (Youden and Mehlich, 1937). It treats a set of distances between sampling locations, which are incremented in geometric progression, as stages in the hierarchy. The central idea of the nested spatial sampling approach is that each stage involves a particular source of variation of the target variable. The contribution of each stage to the overall variance can then be assessed by partitioning the total variance into components. If the variance components for all scales shorter than or equal to a particular length scale are accumulated then the result is an estimate of the variogram with lag distances equal to the length scales (Miesch, 1975).

In the present study, we selected a 120 m by 120 m sized plot (Fig. 1c), which we subdivided into 30 m by 30 m grid cells. Nodal locations of the grid cells constituted the main stations of our nested sampling design, and from them we chose further sampling locations (the substations) at distances of 10 m (substations 1), 3.3 m (substations 2), 1.1 m (substations 3), and 0.36 m (substations 4). According to the requirements of nested spatial sampling, we determined the directions between main stations and substations 1, and between all further substations randomly. Altogether, we took 118 and 111 intact soil cores at the depths of 0–6 cm and 6–12 cm, respectively.

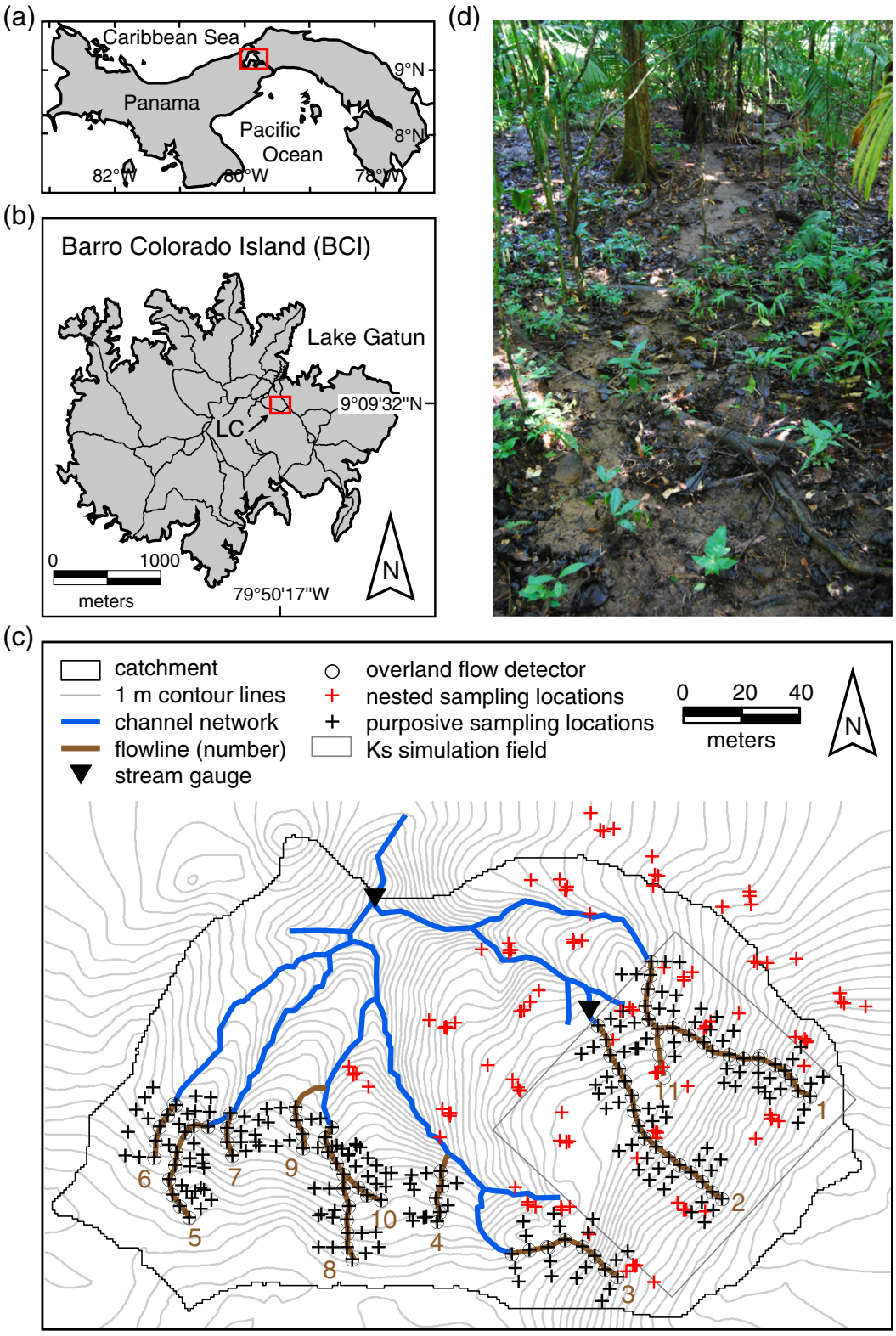

Fig. 1. (a) Location of Barro Colorado Island (BCI) in Panama, and (b) location of Lutzito catchment (LC) on BCI. (c) Map of Lutzito catchment; numbered brown lines refer to flowlines, crosses mark K_s sampling positions and circles depict overland flow monitoring sites. (d) Flowline #2, photograph was taken in the lower part of the flowline after a heavy rainfall event.

2.3.2. Purposive sampling approach

Prior to the purposive sampling campaign we monitored the occurrence of overland flow throughout three consecutive rainy seasons (2007–2009) using overland flow detectors (Kirkby et al., 1976) that we installed in flowlines at regular distances of 5 m. The monitoring started in flowlines that we had identified in the field during rain events (see Video 1, Supplementary material); over the years, ever-increasing field knowledge resulted in the instrumentation of

all major flowlines throughout their entire lengths. The data of this monitoring, which comprised 98 rainfall events, provided the necessary information to determine location, extent and activity of all flowlines in the research area (Fig. 1c). Interestingly, some flowlines nearly reach the catchment divide (e.g. flowline 1, Fig. 1c).

Our purposive sampling strategy involved the collection of soil cores in flowlines, 5 m off flowlines, and 10 m off flowlines; all cores were taken at a depth of 0–6 cm. We dedicated our sampling resources to the upper soil layer where we anticipated the strongest spatial gradient of K_s. In total we sampled 10 of the 11 flowlines under previous monitoring; flowline #11 was excluded because of its vague spatial extent. We determined K_s within flowlines right below the former locations of the overland flow detectors; hence, sampling locations were separated by 5 m distances. The samples outside flowlines were taken perpendicular to the direction of the flowline at both 5 m and 10 m distance to flowline sampling locations. The side (left or right to the particular flowlines) was pre-determined randomly unless major obstacles such as trees, streams or other flowlines precluded the chosen side. In doing so, we took 86 samples within flowlines and another 86 each at distances of 5 and 10 m. The sample size per flowline varied between 3 and 18 depending on flowline length.

2.4. Data analysis

2.4.1. Nested sampling analysis

After an exploratory data analysis including the identification of an appropriate data transformation (cf. Section 3.1), we examined the variance components for each sampling distance using a linear mixed-effects model (Pinheiro et al., 2009). We then accumulated the variance components and calculated the proportion of each component to the total variance. Because the estimation of variance components from a nested spatial sampling is most often accompanied by large uncertainties (Papritz et al., 2011), we did not attempt to interpret these results in terms of physical meaning but rather treated them as a rough indication of the scales over which K_s shows spatial correlation.

2.4.2. Exploratory data analysis of the purposive sample and comparisons with nested sampling data

In this step we compared the three purposively sampled datasets (K_s in flowlines, K_s 5 m off flowlines, K_s 10 m off flowlines) among each other and with the nested sampling datasets by means of box plot comparisons.

2.4.3. Geostatistical model of spatial variation of K_s

The K_s data that we obtained by both nested and purposive sampling in the upper soil layer (0–6 cm depth) can be combined for a geostatistical data analysis. In doing so, we model the spatial variability of the sample data, which can subsequently be reproduced by stochastic simulations. As Lark et al. (2006) state, the geostatistical model of spatial variation is a special case of a linear mixed model where the data are modeled as the additive combination of fixed effects, random effects and independent random error; the latter two are described by the variogram. As suggested by the same authors, we used residual maximum likelihood (REML) to estimate the variogram parameters, whereupon the mixed model equation is solved to estimate the fixed and random effects; the fixed effects can be the unknown mean or the coefficients of a trend model (Lark et al., 2006). For our case study of K_s spatial variation, we ascribed the fixed effects to an external drift variable, the distance to flowline of each point in space, which was calculated on a 1 m grid based on the marked location of the field-determined flowlines. We then applied the t statistic to evaluate the null hypothesis that the coefficients of the trend model are zero; this procedure enables statistical inference about the effect of distance to flowline on the spatial variation of K_s. Since the maximum distance to flowlines of our purposively sampled data is 10 m, we fixed the maximum distance of the drift variable to 10 m, an approach justified a posteriori by our results (cf. Section 3.2).

Any geostatistical analysis requires a proper exploratory data analysis. Both the likelihood estimation of the variogram and sequential Gaussian simulations rely on the assumption of a joint Gaussian data distribution. Whereas this assumption can only be justified theoretically (see discussion in Lark et al., 2006), we can check the uni- and bivariate distribution of the data after appropriate transformation. This was done using histograms and **h**-scattergrams. The **h**-scattergrams are plots of all pairs of measurements which are separated by a fixed distance; they enable us to detect outlying values (Goovaerts, 1997). We assessed the performance of the variogram model by leave-one-out cross-validation and calculated the statistic $\theta(\mathbf{x})$ (Lark, 2000):

$$\theta(\mathbf{x}) = \frac{\left\{z(\mathbf{x}) - \hat{Z}(\mathbf{x})\right\}^2}{\sigma^2{}_{K,\mathbf{x}}}, \quad (2)$$

where $z(\mathbf{x})$ is the observed K_s at location $\mathbf{x}$, $\hat{Z}(\mathbf{x})$ is its kriged estimate, and $\sigma^2_{K,\mathbf{x}}$ is the kriging variance. The mean of $\theta(\mathbf{x})$ is called the mean squared deviation ratio, MSDR (Webster and Oliver, 2001), and should be 1 if the model of the variogram is accurate (Webster and Oliver, 2001). Because outliers in the data will influence $\theta(\mathbf{x})$, we also computed its median, which is 0.455 when a correct variogram is used for kriging (Lark, 2000).

Upon the geostatistical modeling, we used sequential Gaussian simulation (Goovaerts, 1997) to generate sets of values that reproduce the sample statistics while honoring the data at their locations (conditional simulations). Each set of values constitutes a realization of the spatial distribution of K_s, and the use of multiple realizations provides us with a measure of spatial uncertainty (Goovaerts, 1997); if, for instance, most realizations feature certain zones of low K_s we can be confident that these areas actually exist. This is important when we assess the hydrological relevance of the modeled K_s pattern (cf. Section 2.4.4).

2.4.4. Assessment of hydrological relevance

The K_s measurements can be compared to rainfall intensities to get a basic understanding of the hydrological consequences of observed K_s patterns (Chappell and Sherlock, 2005). Since this study is limited to the topsoil, a spatially significant exceedance of K_s by prevailing rain intensities indicates the possibility of overland flow generation.

Rainfall intensities were extracted from a 22-year (1989–2010), 5-min resolution tipping bucket rainfall record from a clearing 250 m away from our study site (rainfall data by courtesy of the Environmental Sciences Program, Smithsonian Tropical Research Institute, Republic of Panama). Because tipping bucket measurements (N_{bucket}) usually underestimate high intensity rainfall, we used complementary totalisator rainfall data of daily resolution (N_{total}, n = 2825 days) for correction of the tipping bucket record ($N_{\text{corrected}}$). Assuming that underestimation starts at a threshold amount per time step (N_{thresh}), above which the measurement error increases linearly with c, we optimized Eq. (4) for N_{thresh} and c to match the daily rainfall record.

$$\sum_{i=1}^{t_{\text{step}}} N_{\text{corrected}}(\text{day}, i) \stackrel{!}{=} N_{\text{total}}(\text{day}) \quad (3)$$

$$N_{\text{corrected}}(\text{day}, i) = N_{\text{bucket}}(\text{day}, i) + \max(0, N_{\text{bucket}}(\text{day}, i) - N_{\text{thresh}}) \cdot c \quad (4)$$

where t_{step} refers to the number of time steps per day.

Based on the corrected tipping bucket data we first selected rain events, which are defined as rainfall periods separated by at least 2 h without rainfall; one-tip-"events" were excluded from the record. We then aggregated six 5-minute readings for events of at least 30-minute duration or all readings for shorter events, respectively. From the aggregated data, we computed the maximum 30-minute rain intensity per event. Last, we selected the minimum, the deciles, and the maximum of these intensities as rainfall thresholds for the comparison with the K_s values.

Our assessment of the hydrological relevance of the K_s data is based on probability statements. First, we evaluated, separately for each dataset, the frequency that a given rainfall intensity exceeds the measured K_s values; high frequencies indicate a spatially significant restraint to vertical percolation. This approach is based on the frequency distribution of the measured K_s values and does inform neither about the spatial extent nor about the continuity of impeding patches, i.e. these patches may be highly localized or spatially clustered. In order to overcome this limitation, we secondly used the geostatistical model to perform 100 conditional simulations on a 1 m grid (cf. Section 2.4.3). These simulations were post-processed to summarize the spatial uncertainty information. We displayed the outcome in probability maps: at each simulated grid cell, the probability of K_s being lower than a given threshold rainfall intensity, is evaluated as the proportion of the 100 simulated values that fall below that threshold (Goovaerts, 1997).

2.4.5. Plausibility check of K_s exceedance probability maps

In the previous step of our analysis we created maps that show the probability of a given rainfall intensity to exceed K_s in each grid cell. To assess the plausibility of these maps we examined the relationship between the probability of K_s exceedance and field data of overland flow occurrence, which we collected for 98 rainfall events (cf. Section 2.3.2). For this analysis we generated probability maps based on the maximum 30-minute rainfall intensity of each of the 98 rainfall events. Because our overland flow monitoring was restricted to flowlines, we extracted only the exceedance probabilities in flowline areas, which were defined as grid cells having a distance to flowline of less than one meter. We then plotted the event-dependent mean probabilities versus the event-dependent fraction of responsive overland flow detectors. A meaningful relationship between probability of K_s exceedance and field data of overland flow occurrence would provide evidence that the simulated K_s data can indeed be used for a rough assessment of the expected extent of (near)-surface lateral flow for given rainfall intensities.

2.4.6. Software

For all calculations, we used the software R, version 2.14.1 (R Development Core Team, 2011). For the nested sampling analysis we applied the package nlme (Pinheiro et al., 2009) and for the geostatistical analysis we used the former package and geoR (Ribeiro and Diggle, 2001).

3. Results

3.1. Nested sampling analysis

Median K_s at 0–6 cm depth is 71.6 mm h^{-1} and drops markedly to 7.3 mm h^{-1} at 6–12 cm depth (Table 1). After transformation to $\log_{10}$, the large coefficients of skewness of the raw data reduce to −0.33 and 0.01 for the datasets from 0 to 6 cm depth and 6 to 12 cm depth, respectively. At 0–6 cm soil depth, the proportions of variance of each sampling stage to the total variance are as follows: 67% of the total variance lay already within the shortest separation distance of 0.36 m, whereas only 3% can be ascribed to values 1.1 m apart. Both the 3.3 m and the 10 m distance resulted in estimated variance components of zero; that is, K_s from measurement locations only 36 cm apart are as different as values 10 m apart. Only the largest separation distance of 30 m yielded a further proportion of 30% to the total variance. At a depth of 6–12 cm, the proportions of variance were determined to be 79%, 19%, 0%, 0%, and 1% for distances of 0.36 m, 1.1 m, 3.3 m, 10 m, and 30 m, respectively. Hence, at both soil depths it is the shortest separation distance of 36 cm which entails the major proportion of the total spatial variability of K_s.

Table 1
Summary statistics of the saturated hydraulic conductivity (K_s) datasets.

Dataset[a]	NS-US	NS-LS	PS-Fl	PS-Fl-5	PS-Fl-10	NS-PS
Depth (cm)	0–6	6–12	0–6	0–6	0–6	0–6
Sample size	118	111	86	86	86	342[b]
K_s (mm h^{-1})						
Minimum	0.18	0.05	0.05	0.06	0.03	0.03
Lower quartile	5.5	0.8	0.9	5.1	13.4	3.3
Median	71.6	7.3	3.8	21.9	79.6	26.4
Upper quartile	312.8	44.2	16.8	56.9	318.2	144.5
Maximum	1691.2	1441.6	278.7	968.6	1692.8	1692.8
MAD[c]	68.8	7.0	3.4	19.9	77.5	25.6
Mean	246.4	77.0	21.5	85.5	233.4	148.7
Std. dev.	393.1	205.9	46.3	165.3	331.0	278.8
Skewness	2.07	4.33	3.60	3.38	2.12	2.93

[a] Datasets are nested sampling in the upper soil layer (NS-US), nested sampling lower soil layer (NS-LS), purposive sampling in flowlines (PS-Fl), purposive sampling 5-m off flowlines (PS-Fl-5), purposive sampling 10-m off flowlines (PS-Fl-10), and combined data of nested and purposive sampling (NS-PS).
[b] 34 data values were excluded due to insufficient quality of geographic coordinates.
[c] MAD refers to the median absolute deviation.

3.2. Exploratory data analysis of the purposive sample and comparisons with nested sampling data

Box plot comparisons reveal a pronounced gradient of K_s with increasing distance to flowlines: median K_s is 3.8 mm h^{-1} in flowlines, increases to 21.9 mm h^{-1} 5 m off flowlines, and eventually approaches 79.6 mm h^{-1} at a distance of 10 m to a flowline (Table 1, Fig. 2). Interestingly, there is a second gradient of K_s (Fig. 3): in proximity to the channel network, that is, in the lower parts of flowlines, K_s values tend to be very low, whereas in the uppermost parts of flowlines K_s values approach those measured at 0–6 cm depth in the nested sampling plot (cf. Figs. 2 and 3). The comparison of purposive and nested sampling datasets show that K_s values in flowlines are not only markedly lower than K_s in the surrounding areas but K_s in flowlines is also similar to K_s measured at 6–12 cm soil depth in the nested-sampling plot (Table 1, Fig. 2). In contrast, K_s data from a 10 m distance to flowlines do not show any difference to the nested sampling plot data from 0 to 6 cm depth (Table 1, Fig. 2).

3.3. Geostatistical model of spatial variation of K_s

The combined data (Table 1) show a large coefficient of skewness (2.93). After transformation to $\log_{10}$ the coefficient of skewness indicates a slight skewness to the left (−0.27) which is acceptable for further geostatistical analyses (Webster and Oliver, 2001). Likewise, the histogram of residuals from the trend model, which we plotted for exploratory purpose, reveals an approximate Gaussian distribution (Fig. 4a), and the **h**-scattergrams do not display outlying values (not shown). Using the maximized log residual likelihood as criterion for model selection, the data are modeled best with an exponential variogram function (Table 2, Fig. 4b). The high nugget-to-sill ratio of 68% corroborates the results of the nested sampling analysis, which attributed most variation to the smallest separation distance. The satisfactory performance of this variogram model (Fig. 4b) is indicated by an MSDR of 0.994 and a median of $\theta(\mathbf{x})$ of 0.486. We subsequently used this model to simulate $\log_{10}$-transformed K_s values within the simulation field (Fig. 1c), which we back-transformed in each realization.

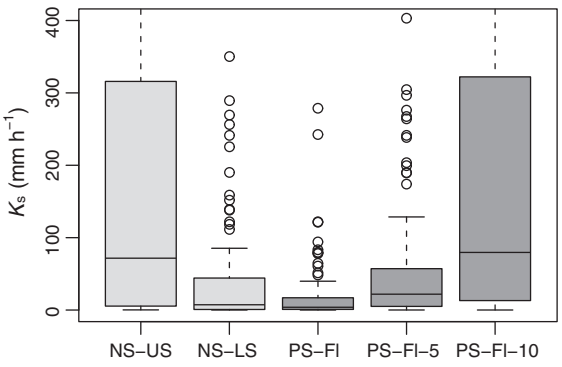

Fig. 2. Box plot comparison of saturated hydraulic conductivity (K_s) data from the two different sampling approaches (only data ≤400 mm h^{-1} are shown): Light gray box plots refer to data from the nested spatial sampling, whereas dark gray box plots show data from the purposive sampling. The abbreviations NS-US and NS-LS refer to the nested sampling in the upper soil layer (0–6 cm depth) and in the lower soil layer (6–12 cm depth), respectively. Abbreviations PS-Fl, PS-Fl-5, and PS-Fl-10 refer to the purposive sampling in flowlines, in 5-m distance to flowlines, and in 10-m distance to flowlines, respectively (all samples were taken at 0–6 cm depth).

The observation of a gradient of K_s with increasing distance to a flowline is supported by the results of the t statistic, which we used to evaluate the null hypothesis that the coefficients of the trend model (Table 2) are zero: fitting a linear trend model to the $\log_{10}$-transformed data (cf. Section 3.3) resulted in a t-value of 2.53 for the intercept (p-value = 0.012, $d.f.$ = 340) and of 8.62 for the slope (p-value = $9 \cdot 10^{-16}$, $d.f.$ = 340), respectively. Hence, we can conclude that the distance to flowline clearly influences the spatial pattern of K_s.

3.4. Assessment of hydrological relevance

Our comparisons of rainfall intensities and K_s, which are based on 8124 rainfall events, clearly show the hydrological relevance of the detected K_s patterns (Fig. 5): if we only considered the nested sampling data at 0–6 cm depth, we would underestimate the influence of topsoil K_s on overland flow generation because even the highest rainfall intensities do not exceed the majority of the K_s values. This impression, however, changes completely if we also consider K_s data from flowlines. In and around flowlines, the potential for overland flow generation increases substantially as high rainfall intensities, e.g. the 0.9 decile of the maximum 30-min rainfall intensity, exceed 80% of flowline K_s values.

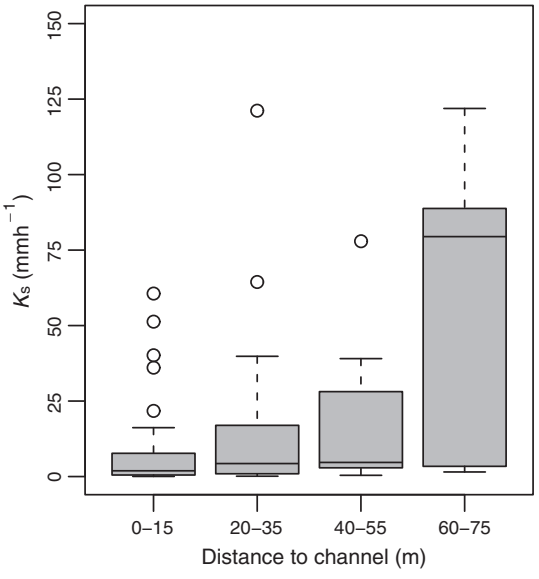

Fig. 3. Box plot comparison of saturated hydraulic conductivity (Ks) measurements grouped into classes of different distances to the channel network. The distance classes 0–15 m, 20–35 m, 40–55 m, and 60–75 m comprise a sample size of 38, 25, 11 and 8, respectively. Two K_s measurements in a distance of >75 m are not included in the comparison. Note: the boxplots are restricted to K_s values ≤150 mm h^{-1}; two larger values, one in the 0–15 m and one in the 40–55 m distance class are not shown.

Our probability maps (Fig. 6) corroborate the findings of the comparisons between the K_s datasets and the range of rainfall intensities (Fig. 5): Flowlines are clearly associated with the highest exceedance probabilities, whereas even the largest rains should percolate vertically through the 0–6 cm soil depth in areas 10 m off flowlines. The probability maps display further interesting issues. Because these maps are based on conditional simulations which use a very large number of data points (cf. Section 2.4.3 and Fig. 6), they do not only reflect the trend of K_s with distance to flowline but also capture a trend of K_s within flowlines (cf. Fig. 3). Due to this feature, increasing rainfall intensities do not simply cause the connection of patches with a high probability of K_s exceedance anywhere in a flowline; instead these patches (i.e. patches in blue) appear first and connect first in the lower parts of the flowlines (cf. maps of the 0.3, 0.4, and the 0.5 decile of maximum 30 min-rainfall intensities, Fig. 6d–f). Moreover, the probability maps reflect a larger spatial trend of K_s with lower values in the downslope area (i.e. the lower part of the maps) and higher K_s values, and hence lower exceedance probabilities, in upslope areas. This trend may reflect a relation between K_s and the topographic wetness index which we calculated with a multiple flow path algorithm. This correlation, however, is weaker than the correlation between K_s and the distance to flowline (R^2 of 0.10 vs. R^2 of 0.19, linear regression model). Further DEM-derived topographic attributes such as single flow path-based topographic wetness indices, slope, upslope contributing area, or flow path length did not show any correlation with our K_s data.

3.5. Plausibility of probability maps

Our comparison between the mean exceedance probability of K_s in flowlines and monitoring data of overland flow response shows that the calculated probability values and field data are related in a meaningful way (Fig. 7a). That is to say, low and high probabilities of K_s exceedance often match the minimum and maximum of overland flow response, respectively. The overland flow response data of 2008, however, cause a large scatter. This is because 2008 was an extremely dry year; in fact, this year ranks as the fifth-driest in the long-term (1929–2010) rainfall record of Barro Colorado Island. As a consequence, soil cracks persisted unusually long during that year and even high intensity rainfalls caused only marginal overland flow (Zimmermann et al., 2012). Overland flow response data of the other years also show some low values, which are as well related to early and mid-wet season events. If we restrict our analysis to late wet season events, the relationship improves; that is, our probability statements of K_s exceedance and field observations match better (Fig. 7b). Even more important than the mere correlation is the fact that overland flow does not start until the mean exceedance probability exceeds a threshold (Zehe et al., 2007) of about 50% and increases steadily from there on. This agreement between exceedance probabilities and measured overland flow occurrence corroborates the suitability of spatial K_s data for an assessment of near-surface flow paths.

4. Discussion

4.1. Spatial variation of saturated hydraulic conductivity: detection of pattern

In the first step of the present study, the nested sampling analysis associated the bulk of K_s spatial variability with the very small

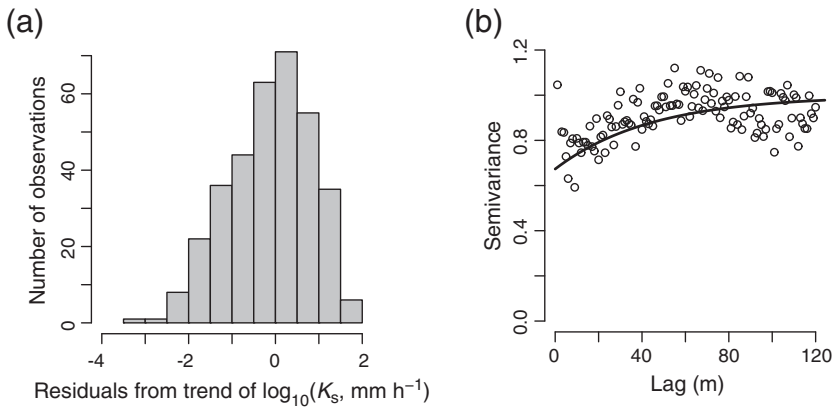

Fig. 4. Histogram of residuals of $\log_{10}$-K_s from the trend model (a) and the experimental variogram of the residuals (b). The line plotted in (b) denotes the variogram model that was fitted by residual maximum likelihood.

separation distance of 0.36 m. Moreover, the variogram model (Fig. 4b), which is based on K_s data of both sampling approaches (cf. Section 2.4.3), also indicates the dominance of small-scale variation (cf. Section 3.3, Table 2). These results are clearly in line with past research findings of areas of homogeneous soil and land cover (Duffera et al., 2007; Mallants et al., 1996; Mohanty et al., 1991; Sobieraj et al., 2004; Zimmermann and Elsenbeer, 2008). The purposive sampling strategy, however, reveals a strong link between the proximity of a sampling point to a flowline and the corresponding K_s value (Table 1, Fig. 2). Therefore, K_s shows a characteristic pattern depending on the topographic position: a large variation of low and high K_s values over short spatial scales prevails in inter-flowline areas (i.e. areas in >10 m distance to a flowline), whereas K_s values in proximity to flowlines tend to be lower due to the distinct gradient of K_s with increasing distance to flowlines (Table 1, Fig. 2). Clearly, this pattern is hard to detect using a sampling approach that focusses on isotropic variation. Therefore, we recommend considering hydrological flow paths during sampling, e.g. ephemeral drainage networks on hillslopes, in order to account for deterministic trends of K_s patterns.

4.2. Spatial variation of saturated hydraulic conductivity: origin of pattern

The short-scale variation of K_s (cf. Section 3.1) and some very high K_s values (Table 1) in inter-flowline areas can be attributed to bioturbation-controlled macroporosity (e.g. Sobieraj et al., 2002). However, the detected deterministic trends, i.e. low K_s in flowlines, a decrease of K_s towards flowlines and towards the channel system into which flowlines drain, have to be explained by another process. We hypothesize that the steady erosion in flowlines (Zimmermann et al., 2012) removed the original topsoil, which is why the uppermost soil layer in flowlines features hydrological characteristics of a lower soil depth. The strikingly similar K_s values in flowlines and in areas without flowlines at a depth of 6–12 cm (Table 1) corroborate this hypothesis. Our field observations indicate that flowlines are not necessarily well defined geomorphic features on hillslopes as they can be relocated by branch and tree falls. The resulting anastomosing of flowlines offers an explanation for the gradual decrease of K_s towards flowlines (Table 1); moreover, it implies that the K_s pattern is not necessarily stable in time. By chance, however, some flowlines have not been subject to disturbance for a long time. In this case, the lowering of K_s towards the flowline can only be explained by occasionally widespread overland flow (e.g. Godsey et al., 2004; Zimmermann et al., 2012) that

Table 2
Results for fitting the geostatistical model by REML.

Trend model:	Linear
Variogram model:	Exponential
Variance model	
Nugget	0.67
Partial sill[a]	0.32
Range[b]	44.13
Fixed effects	
Intercept[c]	0.78 (0.308)
Slope[c]	0.12 (0.014)

[a] Sill variance less the nugget variance.
[b] Distance parameter of the exponential correlation function.
[c] Values in brackets are standard errors.

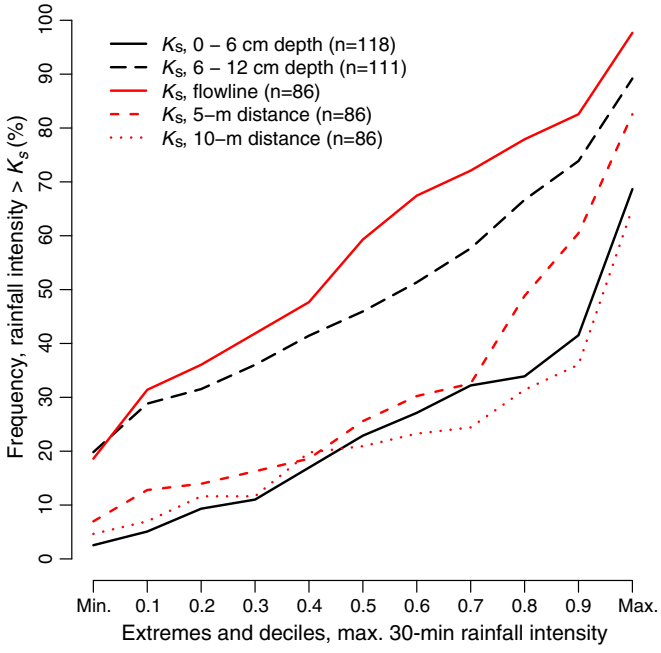

Fig. 5. Frequency of rainfall intensities exceeding saturated hydraulic conductivity (K_s) for the extremes and deciles of the maximum 30-minute rainfall intensity ($maxI_{30}$, n = 8124 rainfall events) and various K_s datasets. The extremes and deciles of $maxI_{30}$ refer to the following rainfall intensities: minimum, 0.6 mm h^{-1}; 0.1 decile, 1.2 mm h^{-1}; 0.2 decile, 1.7 mm h^{-1}; 0.3 decile, 2.3 mm h^{-1}; 0.4 decile, 3.5 mm h^{-1}; median, 5.2 mm h^{-1}; 0.6 decile, 8.1 mm h^{-1}; 0.7 decile, 12.7 mm h^{-1}; 0.8 decile, 21.4 mm h^{-1}; 0.9 decile, 36.4 mm h^{-1}; and maximum, 184.8 mm h^{-1}.

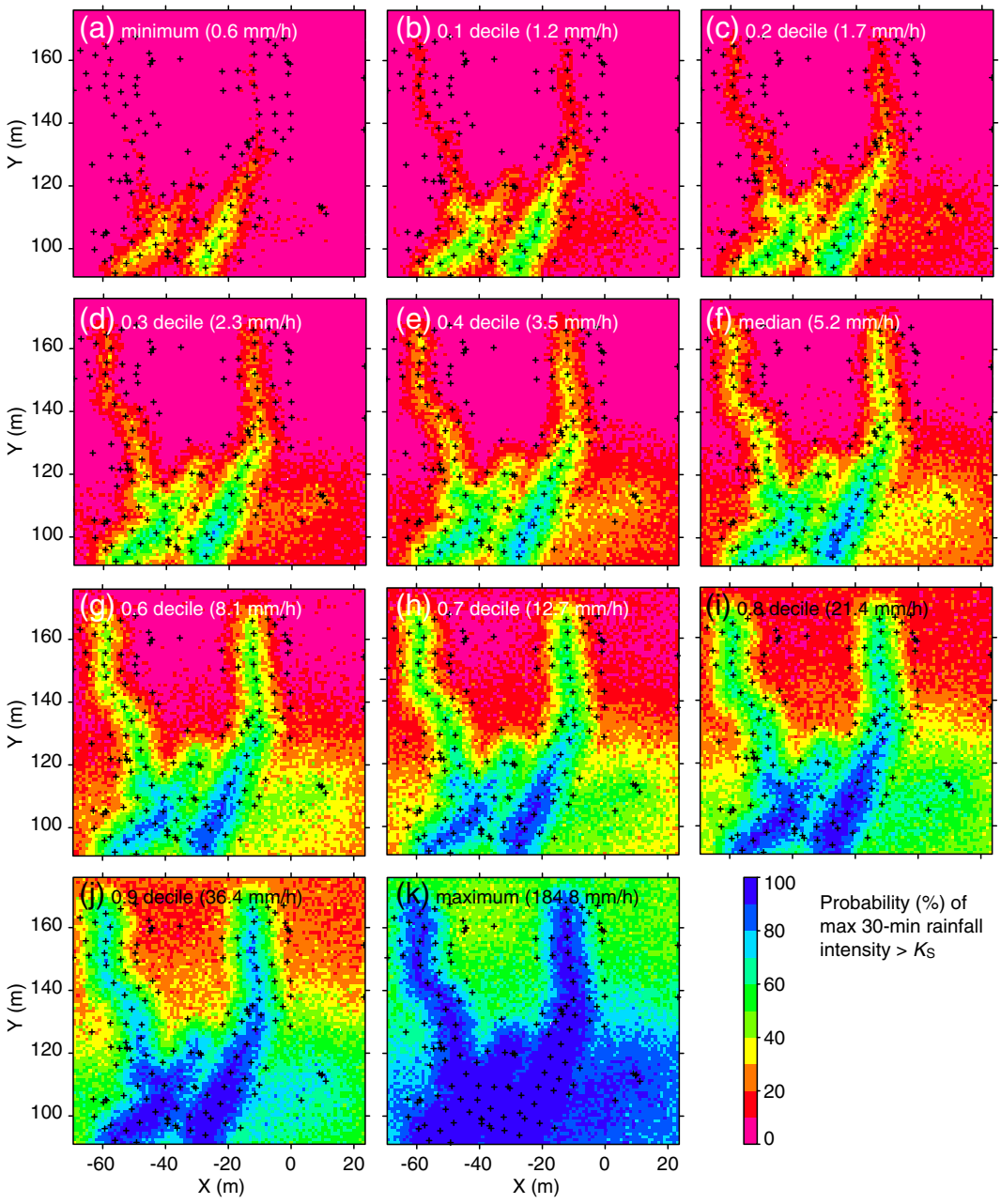

Fig. 6. Probability maps of saturated hydraulic conductivity (K_s) exceedance for the extremes and deciles of the maximum 30-minute rainfall intensity (n = 8124 rainfall events). The maps show an exemplary section of the research area which comprises flowlines 1, 11, and 2 (from left to right, cf. Fig. 1c). The crosses mark sampling locations.

we expect to occur due to the pronounced decrease of K_s with depth: Whereas K_s of the surface soil away from flowlines is too high to be exceeded even by the area's most intense rainstorms (Fig. 6), heavy rainfall has the potential to involve the formation of a perched water table at 6–12 cm depth (Fig. 5) and hence, saturation excess overland flow. With increasing proximity to the flowline, flow increases in depth and so does its erosivity. The increasing depth and frequency of overland flow could also explain the gradient of K_s within flowlines (Fig. 3). According to the above line of reasoning, the development of a flowline provides a typical example of a positive feedback process where the strong decrease of K_s with depth induces a process (saturation excess overland flow) and, subsequently, the development of functional elements (flowlines versus inter-flowline areas) which then produce a pattern (spatial variability of K_s).

4.3. Spatial variation of saturated hydraulic conductivity: hydrological implications

It is remarkable that a variety of studies (Herbst et al., 2006; Merz and Plate, 1997; Mueller et al., 2007) which used very different approaches to derive spatial fields of K_s came to similar conclusions: hydrological predictions based on K_s fields with a distinct, highly organized spatial structure (e.g. connected bands of low K_s) outperform models which apply pure stochastic realizations of K_s. Our results (Figs. 5 and 6) are in line with these findings insofar as the detected deterministic component of the K_s pattern facilitates the understanding of the hydrological response, that is, the high frequency of overland flow in flowlines (Loos and Elsenbeer, 2011; Zimmermann et al., 2012). Yet, the field work necessary to uncover these patterns of K_s is substantial, which is why several studies used auxiliary

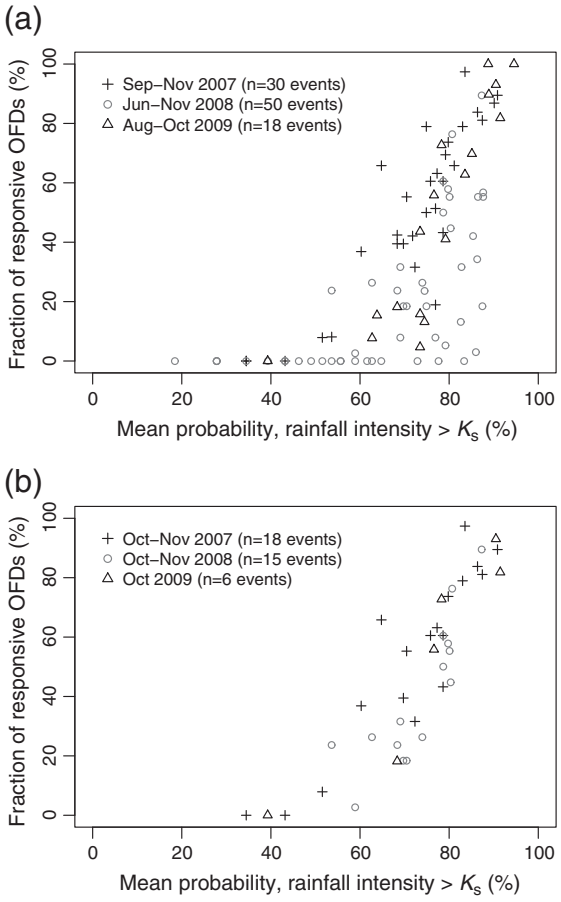

Fig. 7. Fraction of responsive overland flow detectors (OFDs) plotted against K_s exceedance probability in flowlines for a) all monitored events and b) late wet season events only. The probability as given on the x-axis refers to the mean probability that K_s in flowlines is exceeded by a given event's maximum 30-minute rainfall intensity; the mean was calculated from the exceedance probabilities of all flowline grid cells.

variables to generate K_s fields for hydrologic modeling. Merz and Plate (1997), for instance, derived spatially-structured K_s fields by relating K_s to the topographic wetness index. It will not always be possible, however, to link DEM-derived topographic attributes to K_s for two reasons. First, the tremendous small-scale spatial variation of K_s (Fig. 2, Table 1) may mask its possible relationship with topography (Elsenbeer and Vertessy, 2000; Leij et al., 2004). In other words, deterministic trends in K_s patterns are inherently weak and therefore are hard to detect. Second, DEM parameters can be computed in many different ways, and it is known that different algorithms produce strongly varying correlations with environmental variables (Sørensen et al., 2006). In our case, only the application of a multiple flow-direction algorithm reveals the weak correlation between K_s and the topographic wetness index (cf. Section 3.4). Our findings highlight the value of hydrological field data as the distance to flowline parameter captures a larger portion of the variance in K_s than do DEM-derived topographic attributes. As a consequence, our simulations show more distinct patterns of K_s compared with simulated fields based on the topographic wetness index (not shown). Nevertheless, in the absence of information on the spatial extent of active flowlines, the topographic wetness index may serve as an alternative auxiliary variable for implementing deterministic structures into K_s fields.

In spite of the often weak expression of the deterministic trends, their incorporation into spatial fields of K_s helps to understand the hydrological response of the system under study. One way to implement these trends in K_s fields is to use the linear mixed modeling framework as we successfully demonstrated with the distance to flowline as a fixed effect. It is then interesting to link detected K_s patterns to the observed hydrological response of a catchment. In our study we related the probability that K_s is exceeded by a storm's rainfall intensity to observations of overland flow (Fig. 7). This approach revealed the link between the K_s pattern and overland flow occurrence; in addition, by sampling many events at all stages of the rainy season we could demonstrate that the strength of the relationship is not constant but varies over time. During the late wet season, when wetness is highest (Zimmermann et al., 2012), the K_s exceedance probabilities and overland flow response match particularly well (Fig. 7b). During (extremely) dry periods, in contrast, the relationship deteriorates (Fig. 7a) as other processes such the replenishing of the soil moisture deficit and bypass flow in soil cracks possibly dictate the hydrological response of our study area. This varying importance of our simulated K_s pattern for the development of overland flow teaches a general lesson: a sufficient number of rainfall events, which capture the temporal variation of soil hydraulic characteristics, are required to assess the impact of K_s spatial variability on runoff generation.

Finally, our approach to relate K_s patterns and hydrological observations by means of probability maps could be extended further. For instance, we advocate using virtual experiments (Weiler and McDonnell, 2004) as a next step to assess the influence of realistic patterns of K_s on hydrological processes. Such studies could additionally account for the variation in net precipitation (Hopp and McDonnell, 2011) which as a whole may provide valuable insights into the coupling of abiotic patterns at the soil–atmosphere interface.

5. Conclusions

Flowlines, i.e. concentrated flow paths, are common elements in many catchments featuring abundant overland flow. In this study we provide evidence that the saturated hydraulic conductivity (K_s) in the topsoil layer (0–6 cm soil depth) of a forest catchment, which is prone to frequent overland flow, varies as a function of distance to flowline. In flowlines, median K_s in the topsoil layer is low (3.8 mm h^{-1}), increases to 21.9 mm h^{-1} 5 m off flowlines, and approaches a value (79.6 mm h^{-1}) in a distance to flowline of 10 m that resembles K_s of the entire research catchment (median of 71.6 mm h^{-1}). This deterministic component of K_s spatial variation adds to the tremendous small-scale heterogeneity of this soil property. Unfortunately, a sampling approach dedicated to primarily deal with isotropic variation, such as spatial nested sampling, would not suffice to detect the flowline-dependent K_s pattern. Instead, a combined sampling strategy that includes a purposive element based on hydrological field knowledge is required to obtain a realistic description of K_s variation in the investigated high-connectivity landscape. In the absence of information on flowline locations we suggest using the topographic wetness index as an alternative variable for accommodating deterministic trends in K_s.

Surface K_s values in flowlines (3.8 mm h^{-1}) are in the range of catchment-wide K_s at a depth of 6–12 cm (7.3 mm h^{-1}), which suggests that flowlines have been subject to topsoil removal due to steady erosion by overland flow. The decrease of K_s towards flowlines and towards the channel system to which flowlines drain might also be an effect of an increased erosivity due to an increasing depth of flow. We argue that the development of a flowline represents a positive feedback process: the more defined the flowline, the more topsoil is removed, which in turn results in lower K_s values and hence, more runoff.

Based on simulated fields of K_s and prevailing rainfall intensities, we assessed the potential hydrological impact of the detected K_s patterns. If we only considered K_s data from the nested sampling survey, it would seem unlikely that the topsoil layer (0–6 cm soil depth) contributes to surface runoff. This impression changes substantially if we

incorporate the distance to flowline parameter as a fixed effect into our linear mixed modeling framework: In and around flowlines, the potential for overland flow generation increases. We achieved a particular good agreement between probability statements of K_s exceedance and actually measured overland flow occurrence during the wet stages of the rainy season. This highlights the importance of temporal trends in soil hydraulic characteristics for runoff generation. We advocate using more complex virtual experiments for future studies to understand the coupling of abiotic patterns at the soil–atmosphere interface.

Supplementary data related to this article can be found online at http://dx.doi.org/10.1016/j.geoderma.2012.11.002.

Acknowledgments

This research was partially funded by the German Research Foundation (El 255/6-1). Dustin S. Schinn acknowledges support from a German Academic Exchange Service fellowship (D/10/12554), and Helmut Elsenbeer acknowledges support by the Smithsonian Tropical Research Institute during his sabbatical in 2008. Furthermore, we thank Anna Schürkmann, Lena Katharina Schmidt, Simon Plate, and Sophie Godow for participating in the field work, Andreas Papritz (ETH Zürich) for providing the R-code used in the nested sampling analysis, Oris Acevedo (Smithsonian Tropical Research Institute, STRI) for logistical support, and Sergio dos Santos (Environmental Sciences Program, STRI) for providing long-term rainfall data. Finally, we thank two anonymous reviewers for their constructive comments.

References

Ahuja, L.R., Naney, J.W., Gree, R.E., Nielsen, D.R., 1984. Macroporosity to characterize spatial variability of hydraulic conductivity and effects of land management. Soil Science Society of America Journal 48, 699–702.

Baillie, I., Elsenbeer, H., Barthold, F., Grimm, R., Stallard, R., 2007. Semi-detailed soil survey of Barro Colorado Island, Panama. Soil Report ([Online]. Available at http://biogeodb.stri.si.edu/bioinformatics/bci_soil_map/index.php (verified 11 December 2011)).

Bonell, M., Gilmour, D.A., 1978. The development of overland flow in a tropical rainforest catchment. Journal of Hydrology 39, 365–382 http://dx.doi.org/10.1016/0022-1694(78)90012-4.

Bonell, M., Gilmour, D.A., Sinclair, D.F., 1981. Soil hydraulic properties and their effect on surface and subsurface water transfer in a tropical rainforest catchment. Hydrological Sciences Bulletin 26, 1–18 http://dx.doi.org/10.1080/02626668109490858.

Cemek, B., Güler, M., Kilic, K., Demir, Y., Arslan, H., 2007. Assessment of spatial variability in some soil properties as related to soil salinity and alkalinity in Bafra plain in northern Turkey. Environmental Monitoring and Assessment 124, 223–234 http://dx.doi.org/10.1007/s10661-006-9220-y.

Chappell, N.A., Sherlock, M.D., 2005. Contrasting flow pathways within tropical forest slopes of Ultisol soils. Earth Surface Processes and Landforms 30, 735–753 http://dx.doi.org/10.1002/esp. 1173.

de Moraes, J.M., Schuler, A.E., Dunne, T., Figueiredo, R. de O., Victoria, R.L., 2006. Water storage and runoff processes in plinthic soils under forest and pasture in Eastern Amazonia. Hydrological Processes 20, 2509–2526 http://dx.doi.org/10.1002/hyp.6213.

Dietrich, W.E., Windsor, D.M., Dunne, T., 1982. Geology, climate, and hydrology of Barro Colorado Island. In: Leigh, E.G., Rand, S.A., Windsor, D.M. (Eds.), The Ecology of a Tropical Forest: Seasonal Rhythms and Long Term Changes. Smithsonian Institution, Washington DC., pp. 21–46.

Duffera, M., White, J.G., Weisz, R., 2007. Spatial variability of Southeastern U.S. Coastal Plain soil physical properties: Implications for site-specific management. Geoderma 137, 327–339 http://dx.doi.org/10.1016/j.geoderma.2006.08.018.

Dunne, T., Black, R.D., 1970a. An experimental investigation of runoff production in permeable soils. Water Resources Research 6, 478–490 http://dx.doi.org/10.1029/WR006i002p00478.

Dunne, T., Black, R.D., 1970b. Partial area contributions to storm runoff in a small New England watershed. Water Resources Research 6, 1296–1311 http://dx.doi.org/10.1029/WR006i005p01296.

Elsenbeer, H., Vertessy, R.A., 2000. Stormflow generation and flowpath characteristics in an Amazonian rainforest catchment. Hydrological Processes 14, 2367–2381 http://dx.doi.org/10.1002/1099-1085(20001015)14:14<2367::AID-HYP107>3.0.CO;2-H.

F.A.O., 1998. World reference base for soils. World Soil Resources Report, 84. Food and Agriculture Organization of United Nations, Rome, Italy.

Foster, R.B., Brokaw, N.V.L., 1982. Structure and history of the vegetation of Barro Colorado Island. In: Leigh, E.G., Rand, S.A., Windsor, D.M. (Eds.), The Ecology of a Tropical Forest: Seasonal Rhythms and Long Term Changes. Smithsonian Institution, Washington DC., pp. 67–81.

Germer, S., Neill, C., Krusche, A.V., Elsenbeer, H., 2010. Influence of land-use change on near-surface hydrological processes: undisturbed forest to pasture. Journal of Hydrology 380, 473–480 http://dx.doi.org/10.1016/j.jhydrol.2009.11.022.

Godsey, S., Elsenbeer, H., Stallard, R., 2004. Overland flow generation in two lithologically distinct rainforest catchments. Journal of Hydrology 295, 276–290 http://dx.doi.org/10.1016/j.jhydrol.2004.03.014.

Goovaerts, P., 1997. Geostatistics for Natural Resources Evaluation. Oxford Univ., Press, New York.

Grimm, R., Behrens, T., Märker, M., Elsenbeer, H., 2008. Soil organic carbon concentrations and stocks on Barro Colorado Island — digital soil mapping using random forests analysis. Geoderma 146, 102–113 http://dx.doi.org/10.1016/j.geoderma.2008.05.008.

Herbst, M., Diekkrüger, B., Vanderborght, J., 2006. Numerical experiments on the sensitivity of runoff generation to the spatial variation of soil hydraulic properties. Journal of Hydrology 326, 43–58 http://dx.doi.org/10.1016/j.jhydrol.2005.10.036.

Hopp, L., McDonnell, J.J., 2011. Examining the role of throughfall patterns on subsurface flow generation. Journal of Hydrology 409, 460–471 http://dx.doi.org/10.1016/j.jhydrol.2011.08.044.

Iqbal, J., Thomasson, J.A., Jenkins, J.N., Owens, P.R., Whisler, F.D., 2005. Spatial variability analysis of soil physical properties of alluvial soils. Soil Science Society of America Journal 69, 1338–1350 http://dx.doi.org/10.2136/sssaj2004.0154.

Kenoyer, L.A., 1929. General and successional ecology of the lower tropical rain-forest at Barro Colorado Island, Panama. Ecology 10, 201–222.

Kirkby, M., Callan, J., Weyman, D., Wood, J., 1976. Measurement and modelling of dynamic contributing areas in very small catchments. Working Paper No. 167. School of Geography University of Leeds, Leeds (39 pp.).

Lark, R.M., 2000. A comparison of some robust estimators of the variogram for use in soil survey. European Journal of Soil Science 51, 137–157 http://dx.doi.org/10.1046/j.1365-2389.2000.00280.x.

Lark, R.M., Cullis, B.R., Welham, S.J., 2006. On spatial prediction of soil properties in the presence of a spatial trend: the empirical best linear unbiased predictor (E-BLUP) with REML. European Journal of Soil Science 57, 787–799 http://dx.doi.org/10.1111/j.1365-2389.2005.00768.x.

Leij, F.K., Romano, N., Palladino, M., Schaap, M.G., Coppola, A., 2004. Topographical attributes to predict soil hydraulic properties along a hillslope transect. Water Resources Research 40, W02407 http://dx.doi.org/10.1029/2002WR001641.

Loos, M., Elsenbeer, H., 2011. Topographic controls on overland flow generation in a forest — an ensemble tree approach. Journal of Hydrology 409, 94–103 http://dx.doi.org/10.1016/j.jhydrol.2011.08.002.

Mallants, D., Mohanty, B.P., Jacques, D., Feyen, J., 1996. Spatial variability of hydraulic properties in a multi-layered soil profile. Soil Science 161, 167–181 http://dx.doi.org/10.1097/00010694-199603000-00003.

Merz, B., Bárdossy, A., 1998. Effects of spatial variability on the rainfall runoff process in a small loess catchment. Journal of Hydrology 213, 304–317.

Merz, B., Plate, E.J., 1997. An analysis of the effects of spatial variability of soil and soil moisture on runoff. Water Resources Research 33, 2909–2922 http://dx.doi.org/10.1029/97WR02204.

Miesch, A.T., 1975. Variograms and variance components in geochemistry and ore evaluation. Geological Society of America Memoir 142, 333–340.

Mohanty, B.P., Kanwar, R.S., Horton, R., 1991. A robust-resistant approach to interpret spatial-behavior of saturated hydraulic conductivity of a glacial till soil under no-tillage system. Water Resources Research 27, 2979–2992 http://dx.doi.org/10.1029/91WR01720.

Mueller, E.N., Wainwright, J., Parsons, A.J., 2007. Impact of connectivity on the modeling of overland flow within semiarid shrubland environments. Water Resources Research 43, W09412 http://dx.doi.org/10.1029/2006WR005006.

Oliver, M.A., Webster, R., 1987. The elucidation of soil pattern in the Wyre forest of the West-Midlands. England. II. Spatial distribution. Journal of Soil Science 38, 293–307.

Papritz, A., Dumig, A., Zimmermann, C., Gerke, H.H., Felderer, B., Kogel-Knabner, I., Schaaf, W., Schulin, R., 2011. Uncertainty of variance component estimates in nested sampling: a case study on the field-scale spatial variability of a restored soil. European Journal of Soil Science 62, 479–495 http://dx.doi.org/10.1111/j.1365-2389.2011.01363.x.

Pinheiro, J., Bates, D., DebRoy, S., Sarkar, D., R Development Core Team, 2009. nlme: linear and nonlinear mixed effects models. R Package Version 3, pp. 1–92.

R Development Core Team, 2011. R: A Language and Environment for Statistical Computing. R Foundation for Statistical Computing, Vienna, Austria.

Reynolds, W.D., Elrick, D.E., Youngs, E.G., Amoozegar, A., Booltink, H.W.G., Bouma, J., 2002. Saturated and field-saturated water flow parameters. In: Dane, J.H., Topp, G.C. (Eds.), Methods of Soil Analysis, Part 4. Soil Science Society of America, Inc., Madison, pp. 797–878.

Ribeiro Jr., P.J., Diggle, P.J., 2001. geoR: a package for geostatistical analysis. R-NEWS 1, 15–18.

Sobieraj, J.A., Elsenbeer, H., Coelho, R.M., Newton, B., 2002. Spatial variability of soil hydraulic conductivity along a tropical rainforest catena. Geoderma 108, 79–90 http://dx.doi.org/10.1016/S0016-7061(02)00122-2.

Sobieraj, J.A., Elsenbeer, H., Cameron, G., 2004. Scale dependency in spatial patterns of saturated hydraulic conductivity. Catena 55, 49–77 http://dx.doi.org/10.1016/S0341-8162(03)00090-0.

Soil Survey Staff, 2006. Keys to Soil Taxonomy, 10th edition. United States Department of Agriculture, Washington D.C., USA.

Sørensen, R., Zinko, U., Seibert, J., 2006. On the calculation of the topographic wetness index: evaluation of different methods based on field observations. Hydrology and Earth System Sciences 10, 101–112.

Taskinen, A., Sirvio, H., Bruen, M., 2008. Statistical analysis of the effects on overland flow of spatial variability in soil hydraulic conductivity. Hydrological Sciences Journal 53, 387–400 http://dx.doi.org/10.1623/hysj.53.2.387.

Webster, R., Oliver, M.A., 2001. Geostatistics for Environmental Scientists. John Wiley & Sons, Chichester, UK.
Weiler, M., McDonnell, J., 2004. Virtual experiments: a new approach for improving process conceptualization in hillslope hydrology. Journal of Hydrology 285, 3–18 http://dx.doi.org/10.1016/S0022-1694(03)00271-3.
Woodring, W., 1958. Geology of Barro Colorado Island, Canal Zone. Smithsonian Miscellaneous Collections, 135.
Youden, W.J., Mehlich, A., 1937. Selection of Efficient Methods for Soil Sampling: Contributions of the Boyce Thompson Institute for Plant Research, 9, pp. 59–70.
Zehe, E., Elsenbeer, H., Lindenmaier, F., Schulz, K., Blöschl, G., 2007. Patterns of predictability in hydrological threshold systems. Water Resources Research 43, W07434 http://dx.doi.org/10.1029/2006WR005589.
Ziegler, A.D., Giambelluca, T.W., Tran, L.T., Vana, T.T., Nullet, M.A., Fox, J., Vien, T.D., Pinthong, J., Maxwell, J.F., Evett, S., 2004. Hydrological consequences of landscape fragmentation in mountainous northern Vietnam: evidence of accelerated overland flow generation. Journal of Hydrology 287, 124–146 http://dx.doi.org/10.1016/j.jhydrol2003.09.027.
Zimmermann, B., Elsenbeer, H., 2008. Spatial and temporal variability of soil saturated hydraulic conductivity in gradients of disturbance. Journal of Hydrology 361, 78–95 http://dx.doi.org/10.1016/j.jhydrol.2008.07.027.
Zimmermann, B., Zehe, E., Hartmann, N., Elsenbeer, H., 2008. Analyzing spatial data — an assessment of assumptions, new methods and uncertainties using soil hydraulic data. Water Resources Research 44, W10408 http://dx.doi.org/10.1029/2007WR006604.
Zimmermann, A., Francke, T., Elsenbeer, H., 2012. Forests and erosion: insights from a study of suspended-sediment dynamics in an overland flow-prone rainforest catchment. Journal of Hydrology 428–429, 170–181 http://dx.doi.org/10.1016/j.jhydrol.2012.01.039.